# Accepted Manuscript

# International Journal of Applied Mechanics


| | |
|---|---|
| Article Title: | Experimental Studies on Strengthening and Failure Mechanism for the Metal/ Silicone Rubber/ Metal Bonding System |
| Author(s): | Jingchuan Li, Lihong Liang, Xiaoming Liu, Hansong Ma, Jingru Song, Yueguang Wei |
| DOI: | 10.1142/S1758825118500291 |
| Received: | 01 January 2018 |
| Accepted: | 22 February 2018 |
| To be cited as: | Jingchuan Li *et al.*, Experimental Studies on Strengthening and Failure Mechanism for the Metal/ Silicone Rubber/ Metal Bonding System, *International Journal of Applied Mechanics*, doi: 10.1142/S1758825118500291 |
| Link to final version: | https://doi.org/10.1142/S1758825118500291 |






World Scientific
www.worldscientific.com

# Experimental Studies on Strengthening and Failure Mechanism for the Metal/ Silicone Rubber/ Metal Bonding System

Jingchuan Li*,†, Lihong Liang*, Xiaoming Liu*, Hansong Ma*, Jingru Song*

and Yueguang Wei ‡

* *LNM, Institute of Mechanics, Chinese Academy of Sciences, Beijing, 100190, China*

‡ *Department of Mechanics, College of Engineering, Peking University, Beijing 100871, China*

† *College of Engineering Science, University of Chinese Academy of Sciences, Beijing, 100049, China*

‡ *weiyg@pku.edu.cn*

In the present research, we carry out a systematical experimental investigation on the strength, toughness and failure mechanism of the metal/silicone rubber/metal bonding system. For the case of the aluminum alloy cylinder/silicone rubber/aluminum alloy cylinder bonding system, we measure the tensile deformation and failure behaviors, including the dependence of the failure loading on the adhesive layer thickness and scarf angle. Through introducing a series of definitions, such as average normal stress, average shear stress, average normal strain and average shear strain, along the bonding interface, we realize the measurements on interfacial failure strength, and obtain the relationship between the interfacial strength and the interfacial scarf angle as well as adhesive layer thickness, and we further obtain the failure strength surface, interfacial fracture energy, as well as the energy release rate for the bonding system. The obtained results can provide a scientific basis for deeply understanding the strength and toughness properties as well as the failure mechanism of the metal-adhesive bonding system, and have an important guiding for the optimization design and property evolution for the bonding system.

*Keywords*: Metal bonding; adhesive layer thickness; scarf angle; failure strength; interfacial energy.



## 1. Introduction

Metal bonding system has a wide range of applications in the aerospace, marine, automotive and other industrial fields. Compared with the conventional riveting, welding and screw-through connection, the bonding technology has the some advantages that it avoids the high residual stress and deformation concentration within the connection area, which take place in the cases of the riveting, welding and screw-through connection between the metal components, and often lead to stress singularity, crack initiation, crack propagation, and overall fracture. In addition, in ensuring the product performance to meet the needs of the industrial situation, the bonding technology has the advantages of simple manufacturing process, which has attracted widespread industry attention. In simple terms, bonding technology is a method of attaching and fixing a component to another component by using an adhesive, which has the following advantages: (1) stress distribution is uniform and stress concentration coefficient is lower near the joints; (2) the bonding process is easy to be operated, and the bonded structure is light in weight; (3) there are a wide variety of design ideas and a wide range of material selections; (4) bonded structure has good corrosion resistance [Kinloch, 1987]. Therefore, the bonded system has been more and more widely used in the fields of aerospace industry, automobile industry and civil engineering etc. [Wu *et al*., 2002; Dai *et al*., 2005; Ascione, 2009; Grant *et al*., 2009, 2009; Loureiro *et al*., 2010; Higgins, 2000]. In line with the wide range of applications and industrial applications, people have conducted extensive researches on the toughness properties of bonded systems in recent decades, and have done a great deal of research on the properties of adhesives and the development of new adhesives. For example, the properties of adhesives with fillers [Kahraman *et al*., 2008], the bonding behavior of different adhesives [Afendi *et al*., 2011, 2013], the application of bonded systems in special environments such as humidity [Goglio *et al*., 2009] and high temperatures [Banea *et al*., 2014].

‡Corresponding author

The remarkable advantage of the bonded system is that its combined interface has good toughness characteristics. Effectively delineating this toughness mechanism is crucial for designing new bonded systems for product updates. However, the strength and failure behavior of bonded systems are difficult to be clearly characterized because of the complicated stress state of the bonded interface layer [Afendi *et al*., 2011, 2013; Wang *et al*., 1997; Imanaka *et al*., 2000]. Previous studies mainly focused attentions on the toughness and failure mechanisms of bonded systems from both experimental and computational simulations. The stress distribution in the layers, the stress concentration at the edge of the interface and the mechanical properties of bonded system under complex loading conditions were widely studied. In experimental studies, a mixed loading system (called modified Arcan sample) is commonly used to measure the interfacial fracture behavior of bulk bonded specimens under pull-shear or pressure-shear mixing loading conditions [Arcan *et al*., 1987; Stamoulis *et al*., 2016; Choupani, 2008a, 2008b]. The scarf joint specimens are used to measure the interfacial fracture behavior [Afendi *et al*., 2011, 2013]. People investigated the strength and failure characteristics of bonded systems under different loading conditions, such as bending [Nakano *et al*., 2013; Liao *et al*., 2014], impact [Kim *et al*., 2012], fatigue [Jen *et al*., 2012; Zhan *et al*., 2017], and so on. Nakano and Sekiguchi [Nakano *et al*., 2013] studied the bending load case for the scarf joints, they found that when the adhesive layer thickness was reduced or the Young's modulus of the adhesive was increased, the stress at the edge of the interface was reduced and the strength of the joint was increased. They also found that when the scarf angle was around 60 degrees, the maximum bending moment was corresponded. People also studied the stress distribution [Nakano *et al*., 2013, 2014] and the stress concentration [Afendi *et al*., 2011] in the vicinity of the adhesive layer. Afendi and Teramoto [Afendi *et al*., 2013] designed the scarf joints of different types of adherend at both ends of the glue layer to study their strength and failure. Through experimental measurements and finite element numerical simulations, they found that the stress concentration was most prominent at the corner of the interface between the steel and the adhesive, from where the crack began to transition to the corner of the interface between the aluminum and the adhesive at the other end. They regarded the corner as a 90-degree crack of interface and defined the interface corner toughness [Groth, 1988], which was further used to characterize the strength of the adhesive, and the results were in good agreement with the experiment. Their experimental observations also showed that the failure of the joints often started at the free boundary. Some scholars used the double scarf joints [Liao *et al*., 2014; Gacoin *et al*., 2009] and modified scarf joints [Bendemra *et al*., 2015]. Gacoin *et al*. [Gacoin *et al*., 2009] investigated the effect of the singularities generated by the internal geometry of the double scarf joint on the damage evolution of the bonded joints. They found that when the specimen was subjected to axial tensile loading and the scarf angle was greater than 18 degrees, the initiation of initial cracks will be limited. There has been a great deal of researches on scarf joints, mainly involving stress analysis in bonded joints and the prediction of joint failure strength. Some scholars used two-dimensional model to study the stress state and strength prediction of scarf joints under static load [Suzuki, 1985, 1987]. Some scholars used three-dimensional model to study the stress singularity at the edge of scarf joints [Chaudhuri *et al*., 2009; Chiu *et al*., 2011]. Xu Wei *et al*. [Xu *et al*., 2012] introduced the destructive mechanism and influencing factors of the bonded interface in their review articles, and summarized the research status on the scale effect of the adhesive layer. Zhang *et al*. [Zhang *et al*., 2016] used two kinds of brittle and ductile adhesives, respectively, the bonded butt specimens were pulled or sheared to rupture. Li *et al*. [li *et al*., 2013] studied the effects of various metal surface pretreatment methods on the bond strength of polymers using pull-shear experiments. Wang *et al.* [Wang *et al*., 2017] reviewed the research status of the interface strength and corrosion resistance of aluminum alloy joints from the aspects of aluminum alloy surface roughness, microstructure, surface oxide layer and coating chemical properties.

Although a great deal of researches have been conducted on the toughness mechanism of bonded systems and some phenomena and laws have been revealed, it is still necessary to conduct a systematic and in-depth study on bonded systems, especially the mechanism of combined interfaces. Previously, in studying the toughness mechanism of the bonded system, the predominantly prismatic samples are used to be adopted. The results undoubtedly depend more on the stress singularity effect in the vicinity of the edge of the combined interface. This kind of the stress singularity effect is very sensitive to the bond

quality of the adhesive layer, which greatly increases the complexity in understanding bonding mechanism from the experimental results.

In order to eliminate the stress singularity effect, in the present research we adopt a new kind of samples, i.e., cylindrical bonding samples, and we shall focus on the toughness mechanism of the combined interface to investigate the toughness and failure mechanism of the bonded system of the aluminum alloys bonded by silicone rubber, which are commonly used in the field of industry such as aerospace. Compared with the common rectangular cross-section specimens, the stress singularity effect of the non-edge cylindrical specimens is very weak, so pure interface adhesive characteristic will be clearly revealed. Experiments will be carried out on samples with different scarf joints and adhesive layer thicknesses. The experimental results are then analyzed to obtain the characterization of the toughness mechanism of the bonded system, and then the failure criterion of the bonded system will be developed.

## 2. Experimental Program and Experimental Process

In order to model the toughness performance of commonly used bonded parts in the field of aerospace, in the present research, we select a bonded system as aluminum alloy/silicone rubber/aluminum alloy, and carry out a systematic experimental research. The basic mechanical properties of aluminum alloy (2A12-CZ) is shown in Table 1. The adhesive, silicone rubber (704 produced by Jiangsu Nanda Co., China) is a ductile adhesive [Yang *et al*., 2014], and its mechanical properties are tabulated in table 2, where, $E$, $\sigma_s$ and $v$ are Young's modulus, 0.2% proof stress and Poisson's ratio, respectively, measured based three samples. Tensile specimens are prepared according to international standards, and the force displacement curve is obtained by quasi-static loading. Then the corresponding mechanical parameters are calculated. The maximum tensile and shear strengths of the silicone rubber standard specimens are 0.33 MPa and 0.55 MPa [Yang *et al*., 2014], respectively. It is a kind of ductile adhesive widely used for sealing, coating and bonding of small components. It can be seen that the modulus of the adherent aluminum alloy 2A12-CZ (about 70GPa) is about 50 thousand times that of the silicone rubber (Table 2 for the present study), and the deformation is relatively small throughout the destruction of the sample.

The geometry of the scarf joint specimens is shown in Figure 1. Wherein the black part is silicone adhesive layer, adherends at both ends of the adhesive are aluminum alloys. The cross section is circular, and the adherends are perforated at both ends to facilitate loading. The diameter of the sample, the overall length (except adhesive adhesive) and the holes remain unchanged, where $t$ is the thickness of the adhesive layer, the range of variation is 0.1–0.6mm, $\theta$ is the scarf angle of the adhesive layer, which can be selected as the range of 0–75 degree in this study.

Table 1. Mechanical property parameters of aluminum alloy.

| Alloy | Dimension (mm) | Tensile Strength (MPa) | Yield Strength (MPa) | Elongation (%) |
|---|---|---|---|---|
| 2A12-CZ | 19 | 560–565 | 440–460 | 14–16 |

Table 2. Mechanical property parameter of silicone rubber.

| Type of adhesive | Sample Number | $E$ (MPa) | $\sigma_s$ (MPa) | $v$ |
|---|---|---|---|---|
| Silicone rubber | 1 | 1.33 | 0.036 | 0.4 |
| | 2 | 1.60 | 0.043 | 0.4 |
| | 3 | 1.60 | 0.048 | 0.4 |

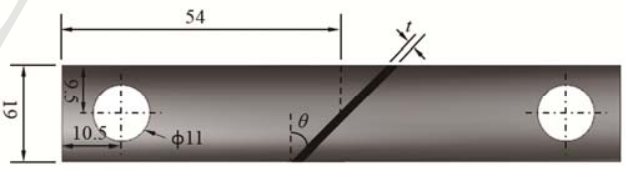

Fig. 1. Specimen size (mm).

Before bonding, the aluminum alloy is immersed in absolute ethanol with ultrasonic cleaning machine for 5 minutes to remove oil, sediment and other debris. Rinse out under water flow, polish the surface of the aluminum alloy rods with # 600 sandpapers, and wear the marks parallel to the minor axis of the bonding ellipse to achieve better interface bonding. After polishing with clean ethanol in the ultrasonic cleaning machine for five minutes, use a blower to blow cold air to remove residual liquid, immediately followed by the bonding step.

In order to ensure the intended target bond thickness $t$, the adhesive layer is controlled by two copper wires with a length of 8 mm and a diameter of $t$, and the copper wire is arranged in the same direction as the polishing direction. A kind of fast solidification glue (Ethyl cyanoacrylate) is used to fix the copper wires onto the central region of the adherend to prevent sliding during the process of curing. This approach refers to the method of Yang *et al*. [Yang *et al*., 2014]. Since the volume of copper wire is extremely small relative to the volume of the entire adhesive layer and the area of contact between the copper wires and the metal rods is extremely small relative to the area of the entire adhesive layer and the cross-section of the metal rod, Yang *et al*. [Yang *et al*., 2014] proved that the presence of copper wires has insignificant effect on bond strength. In order to get better specimens, some specially developed fixtures with semi-circular grooves are used to hold cylindrical joints. Apply the adhesive evenly to the surfaces of both aluminum alloys adherends. The corresponding parts of the two adherends are superimposed on the mold with the cling film placed in advance, to prevent the adhesive and mold bonding. Then squeeze excess adhesive, buckle with the other half of the mold, and use a lead block to apply pressure outside the mold until fully cured. Curing for about 60 minutes, the sample curing positioning, carefully moved to 25 ℃ incubator for 24 hours to achieve complete cure. After the sample is completely cured, the cling film is removed, the excess glue is removed with a cutter, and the actual average thickness of the adhesive layer is shown in Table 3. As can be seen from Table 3, the actually obtained thickness of the adhesive layer is slightly thicker than the thickness of the target bond thickness. Especially for the samples requiring a relatively thicker adhesive layer and a larger scarf angle, the difference between the actual thickness and the target thickness is relatively larger, but the error can be maintained within 10% of the range. In order to systematically study the mechanical properties of the bonding interface of metal / silicone rubber / metal bonding system and reveal the mechanical properties of the system, In the experimental study, we focused on five different representative bond thickness (0.1mm, 0.2mm, 0.3mm, 0.4mm and 0.6mm) and six representative scarf angles (0°, 15°, 30°, 45°, 60°, 75°). In order to get reliable experimental results, each type of sample is prepared more than three. It is worth of noting that in the following discussions, we directly get the load-displacement curves, instead of presenting the data in the table because the failure loads will be concerned about in the present research. Tensile testing is performed on a multi-purpose material testing machine with a load rate of 0.1 millimeter per minute. For each kind of sample geometry, three times experiments are performed.

Table 3. The measured average adhesive layer thickness.

| $\theta$(°) | $t$ (mm) | | | | |
|---|---|---|---|---|---|
| | 0.1 | 0.2 | 0.3 | 0.4 | 0.6 |
| 0 | 0.11 | 0.22 | 0.32 | 0.43 | 0.64 |
| 15 | 0.11 | 0.21 | 0.32 | 0.43 | 0.63 |
| 30 | 0.12 | 0.22 | 0.32 | 0.43 | 0.63 |
| 45 | 0.11 | 0.21 | 0.32 | 0.43 | 0.63 |
| 60 | 0.11 | 0.22 | 0.32 | 0.43 | 0.63 |
| 75 | 0.11 | 0.22 | 0.33 | 0.42 | 0.63 |

## 3. Tensile Load-Displacement Curves of Aluminum Alloy/ Silicone Rubber/ Aluminum Alloy Bonding System

### 3.1. *Load - displacement curves*

In the present research, we investigate the strength and fracture energy of the bonded system with the variations of both adhesive layer thickness and scarf angle. In order to avoid the large number of experiments involved and to check the repeatability of test results, we adopt three samples for each sample size. The representative result shown in Figure 2 corresponds to the case where the thickness of the adhesive layer is $t$ = 0.3 mm, and the scarf angle is 15° . For each scarf angle and each bond thickness, three sample experiments show three force displacement curves, respectively, shown in the Figure 2 labeled 1,2,3. It can be seen from the Figure 2 that the aluminum alloy/ silicone rubber / aluminum alloy system samples show ductile fracture characteristics. As the displacement increases, the load-displacement curve first shows an approximate linear elastic relationship, and then a non-linear relationship. When the load increases to a maximum value, the sample suddenly breaks down, the crack is significantly expanded, and adhesive failure is taken place within the bonding layer. After the obvious decline, we can see the decline tends to be gentle. The experimental results of the three samples have a certain dispersibility, failure load difference does not exceed 20%. Displacement difference is also about 20%. In the ensuing discussion, the curve centered on the value of the load-displacement curve in the three specimens is analyzed (the red line in Figure 2. The dispersion of the experimental results is not particularly prominent). The selection of the curve will be given in the following analysis for the specific instructions.

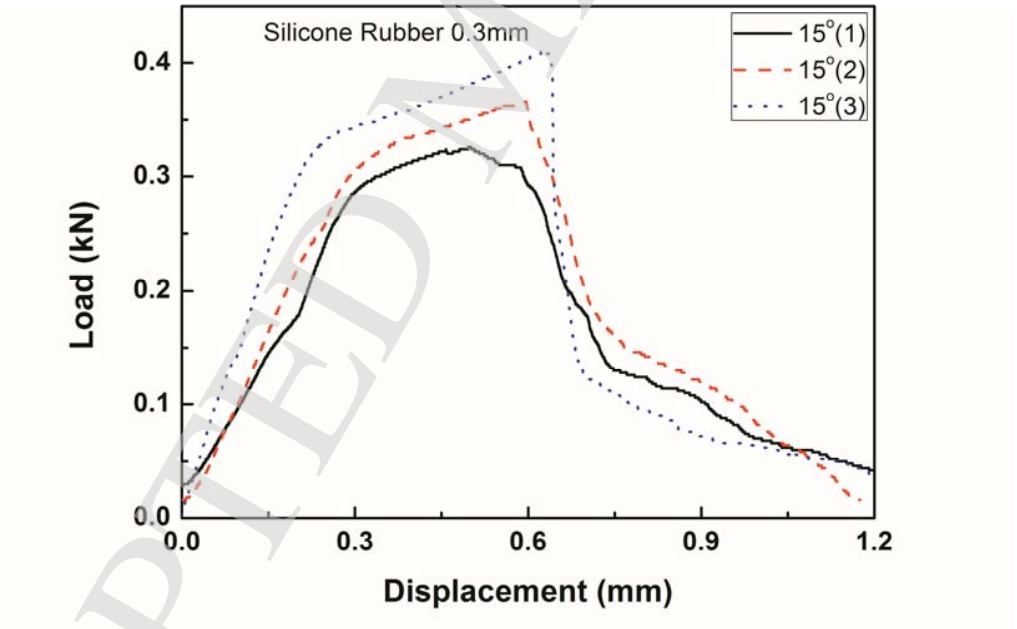


Fig. 2. Load-displacement curve of typical specimen of the aluminum alloy/ silicone rubber/ aluminum alloy

A large number of load-displacement curves have been obtained in experiments, which are divided into two categories, corresponding to the given bonding scarf angle to change the thickness of the adhesive layer and given the thickness of the adhesive layer to change the bonding interface angle, respectively. Figure 3 shows the results for a given adhesive layer thickness changing scarf angle where the layer thickness is $t$ = 0.2 mm. It can be seen from Figure 3 that the load-displacement curves

obtained by the samples with different scarf angles are similar in shape, and the failure load increases as the scarf angle increases. The slope of the load-displacement curve of the 45 degree specimen is the lowest, and the slope of the load-displacement curve of the 0 degree and 75 degree specimens is relatively high. Other adhesive layer thickness of 0.1–0.6mm also have similar changes in the law. It should be noted that: Figure 3 corresponds to a variety of experimental results of the scarf angle, in order to facilitate the comparison of experimental curves in different situations, we plotted the results for each of the three specimens (see Figure 2) with only the middle of the numerical values plotted in Figure 3 to allow for a comparison of the deviations of results between different scarf angles.

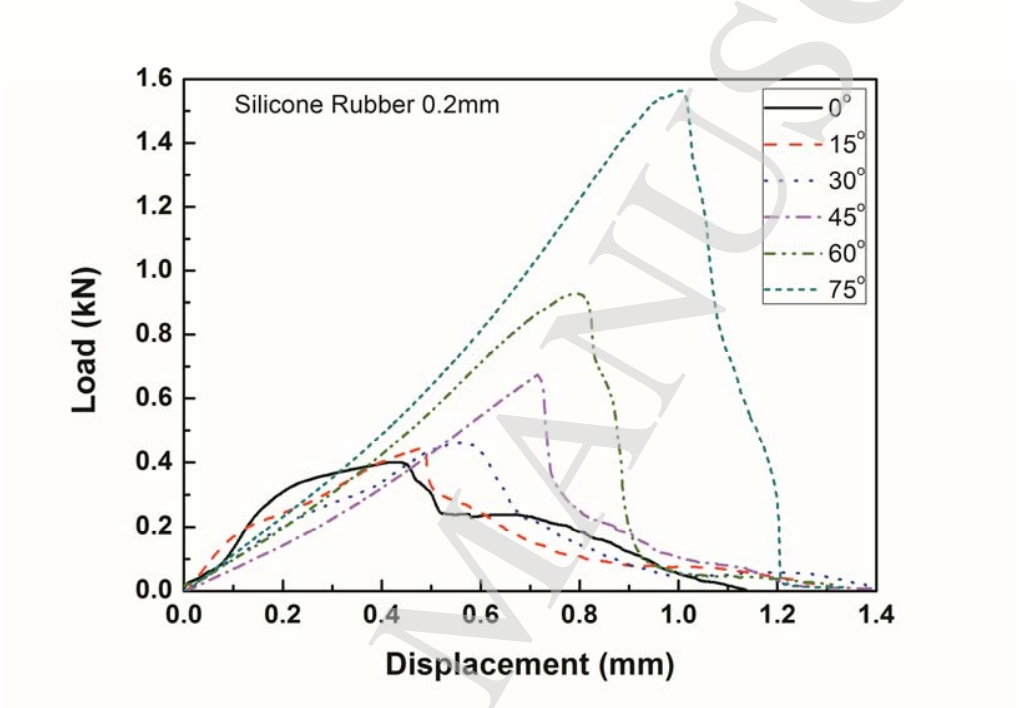


Fig. 3. Load-displacement curves for varying angle of adhesive interface and given adhesive layer thickness.

Figure 4 gives the load-displacement curve for the change in the scarf angle for a given bonded interface angle, corresponding to a case where the scarf angle is 45 degrees. It can be seen from the Figure 4 that the maximum load value is sensitive to the change of the thickness of the adhesive layer, and the shape of the load-displacement curve to the change of the thickness of the adhesive layer is complicated, especially after the maximum load points or for the case of small scarf angles (referring to Figure 3). For thick specimens before destruction, there is a curve where the displacement increases but the load remains essentially constant, showing a certain ductile characteristics. Both the ultimate failure load and the slope of the load-displacement curve decrease obviously with the increase of the thickness of the adhesive layer, and have a strong scale effect on the thickness of the adhesive layer. The limit displacement value changes slightly. It should be noted that: Figure 4 corresponds to a variety of experimental results of the bond thickness, in order to facilitate the comparison of experimental curves in different situations, we plotted the results for each of the three specimens (see Figure 2) with only the middle of the numerical values plotted in Figure 4 to allow for a comparison of the deviations of results between different bond thickness.

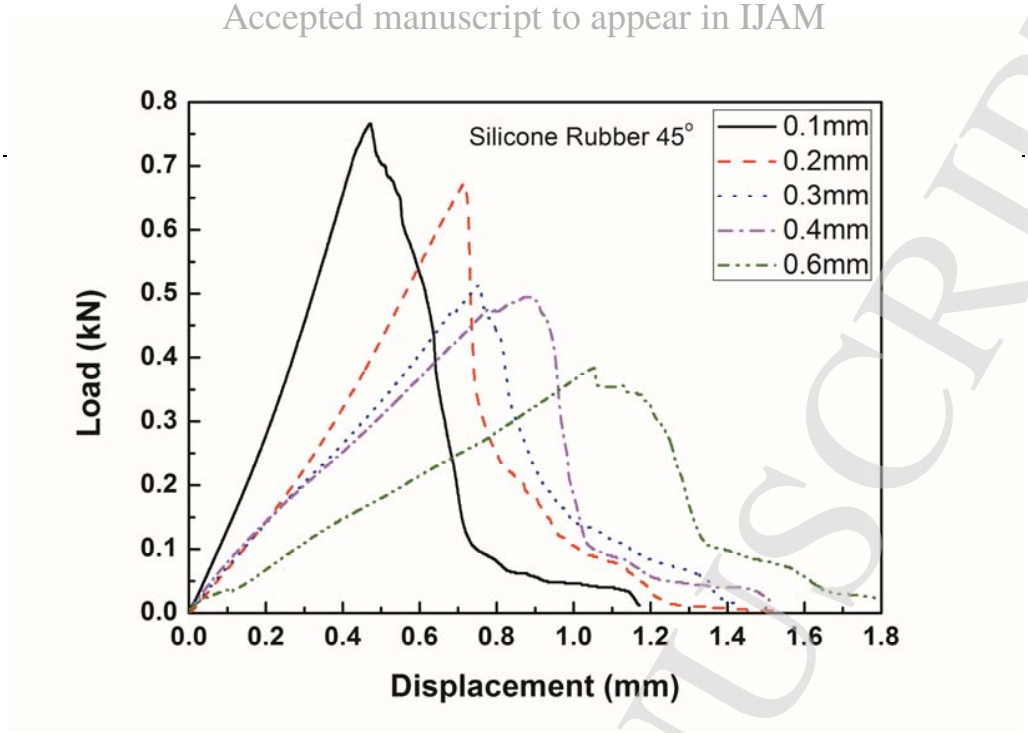


Fig. 4. Load-displacement curves for varying adhesive layer thickness and given angle of adhesive interface.

### 3.2. *Failure load curves*

Figure 5 shows the relationship between the ultimate load and the change of the scarf angle. The different curves correspond to different adhesive layer thicknesses, and the error bars correspond to the results of three specimens with same adhesive layer thicknesses and the scarf angles. As can be seen from the Figure 5, the failure load of specimens with different bond thickness keeps the same regularity as the scarf angle changes. When the scarf angle changes from 0 degree to 45 degrees, the failure load increases slowly, but as the angle continues to increase, the failure load increases dramatically, which is similar with bonding area changing with scarf angle. The thinner the adhesive layer thickness, the higher failure load is. It can be seen from the Figure 5 that the failure load has obvious scale effect on the thickness of the adhesive layer thickness.

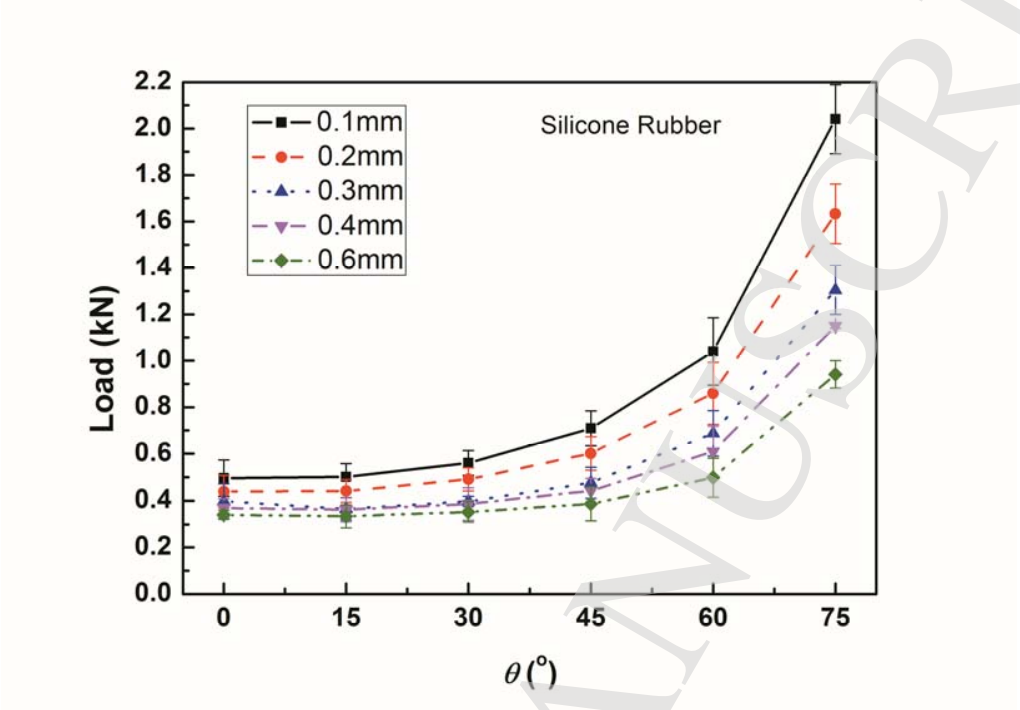


Fig. 5. Failure loads vary with scarf angle

## 4. Interface Strength of the Aluminum Alloy/ Silicone Rubber / Aluminum Alloy System

In Figure 3–Figure 5, we have shown the load-displacement curves and the failure load-interface adhesive angle curves for the aluminum alloy/ silicone rubber / aluminum alloy bonding system and for different adhesive layer thickness. Since the elastic modulus of the aluminum alloy is much higher than the elastic modulus of the silicone rubber, it can be approximately assumed that the tensile deformation mainly occurs in the adhesive layer, and tensile fracture occurs in the adhesive layer. Based on the results of Figure 3–Figure 5, we can obtain the interface strength of aluminum alloy / silicone rubber / aluminum alloy samples. The stress state in the adhesive layer can be approximated as a mixed mode of uniform tension perpendicular to the interface and simple shear parallel to the interface. So we can decompose the previously obtained load-displacement curve into the relationship between average normal stress and average normal strain and the relationship between average shear stress and average shear strain along the bonding interface. We can further obtain a failure law and a fracture energy law for the bonded system.

Referring to the mechanism of average stress and deformation geometry of the bonding interface, as shown in Figure 6, the average normal stress $\bar{\sigma}$ and the average shear stress $\bar{\tau}$ along the bonding interface can be expressed as

$$\bar{\sigma} = \frac{F}{A}\cos^2\theta \tag{1}$$

$$\bar{\tau} = \frac{F}{2A}\sin 2\theta \tag{2}$$

where $F$ is the tensile load, $A$ is the cross-sectional area and $\theta$ is the scarf angle.

The average normal strain $\bar{\varepsilon}$ and the average shear strain $\bar{\gamma}$ along the bonded interface are as follows

$$\bar{\varepsilon} = \frac{d\cos\theta}{t} \tag{3}$$

$$\bar{\gamma} = \frac{d \sin\theta}{t} \tag{4}$$

where $d$ is the total tensile displacement.

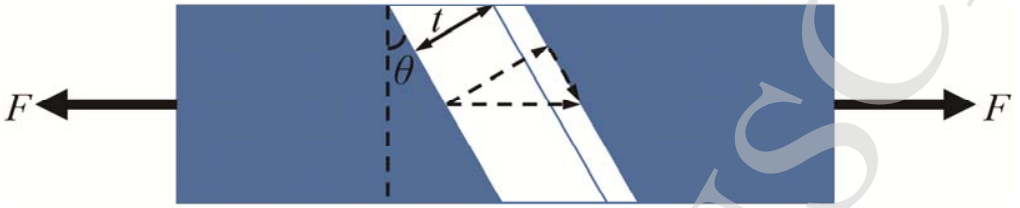


(a)

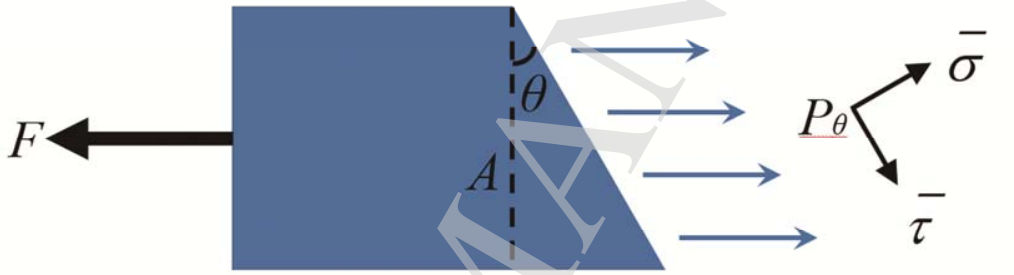


(b)

Fig. 6. Sketch Figures of deformation and average stresses on the adhesive interface. (a)Sketch of deformation; (b)Sketch of average stresses.

From experimental load-displacement curves shown in Figure 3 and the formulas (1) –(4), we can get the experimental relationship between the average normal stress and the average normal strain for the bonded interface, as shown in Figure 7 (a). Simultaneously, we also get the experimental relationship between the average shear stress and the average shear strain for the bonded interface, as shown in Figure 7 (b). The results correspond to the case where the silicone rubber adhesive layer thickness is $t$ = 0.3 mm, and 6 scarf angles are from 0 degree to 75 degrees. The slope of the elastic section of the average normal stress- strain curve and the average shear stress- strain curve are equal, which decrease with the increase of the scarf angle. This can be seen clearly from formulas (1) –(4). The maximum average normal stress decreases with the increase of the scarf angle, and the maximum average shear stress increases with the increase of the bonding interface angle. It can be seen that as the scarf angle increases, the interface failure of the bonded system changes from the tensile-dominated failure to the failure of simple shear-dominated fracture. Other case of adhesive layer thickness has a similar rule. It should be noted that Figure 7 corresponds to a variety of experimental results of the scarf angle, in order to facilitate the comparison of experimental curves in different cases, we plot the results for two specimens of the three specimens without middle one of the numerical values to allow for a comparison of the deviations of results between different scarf angles.

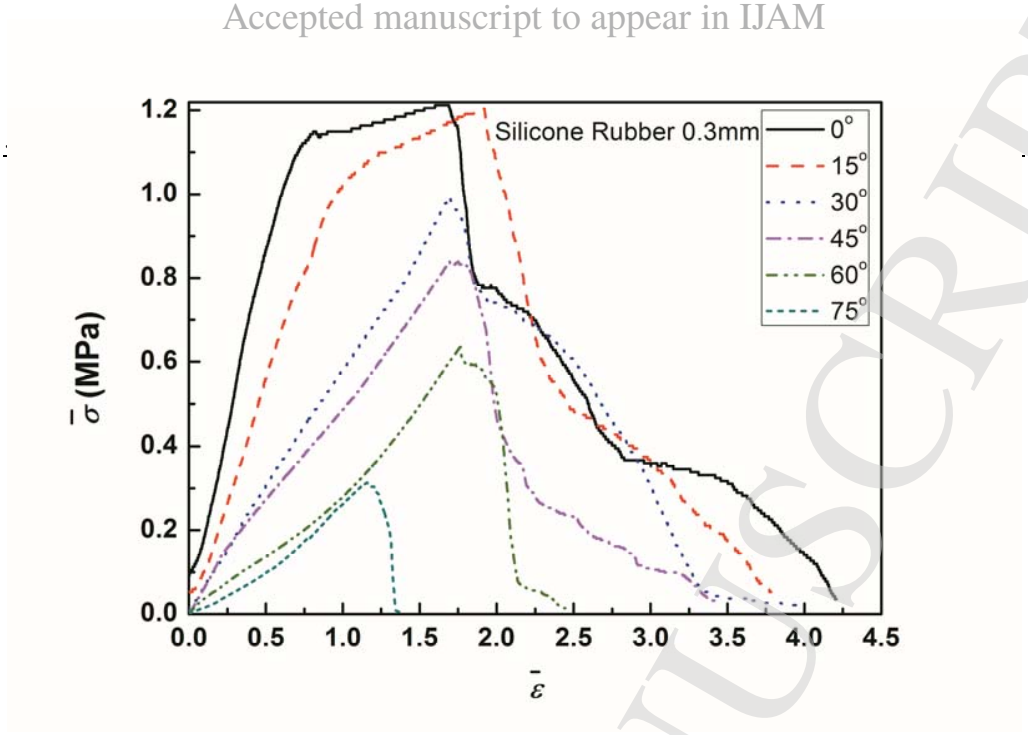


(a)

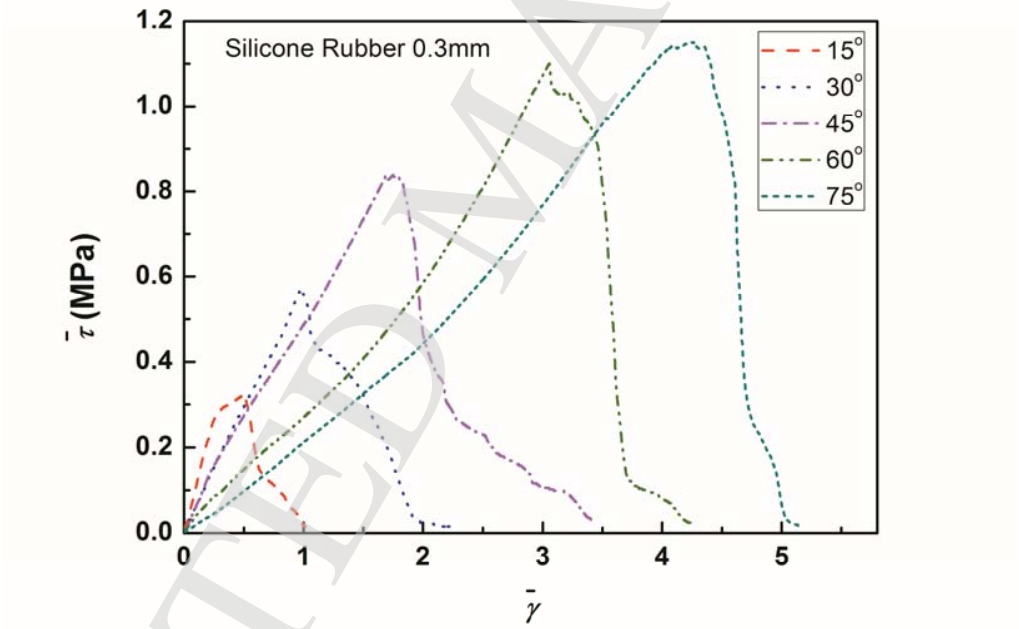


(b)

Fig.7. Relations of average stress and average strain for varying angle of adhesive interface and given adhesive layer thickness. (a)Average normal stress vs average normal strain; (b) Average shear stress vs average shear strain.

Similarly, from experimental load-displacement curves shown in Figure 4 and the formulas (1) –(4), we can get the experimental relationship between the average normal stress and the average normal strain for the bonding interface. At the same time, we can also get the experimental relationship between the average shear stress and the average shear strain for the bonding interface. The corresponding scarf angle is 45 degree and the thickness of the adhesive layer is 0.1mm–0.6mm situation. In Figure 8, we give the average normal stress-average normal strain curves of the bonded interface with the scarf angle of 0 degree. As can be seen from Figure 8, the slope of the average normal stress-average normal strain curve changes slightly with the change of the adhesive layer

thickness. The maximum average normal stress decreases as the adhesive layer thickness increases. Other scarf angle cases have the similar trends, that is, both the maximum average normal stress and the maximum average shear stress increase with decreasing the adhesive layer thickness.

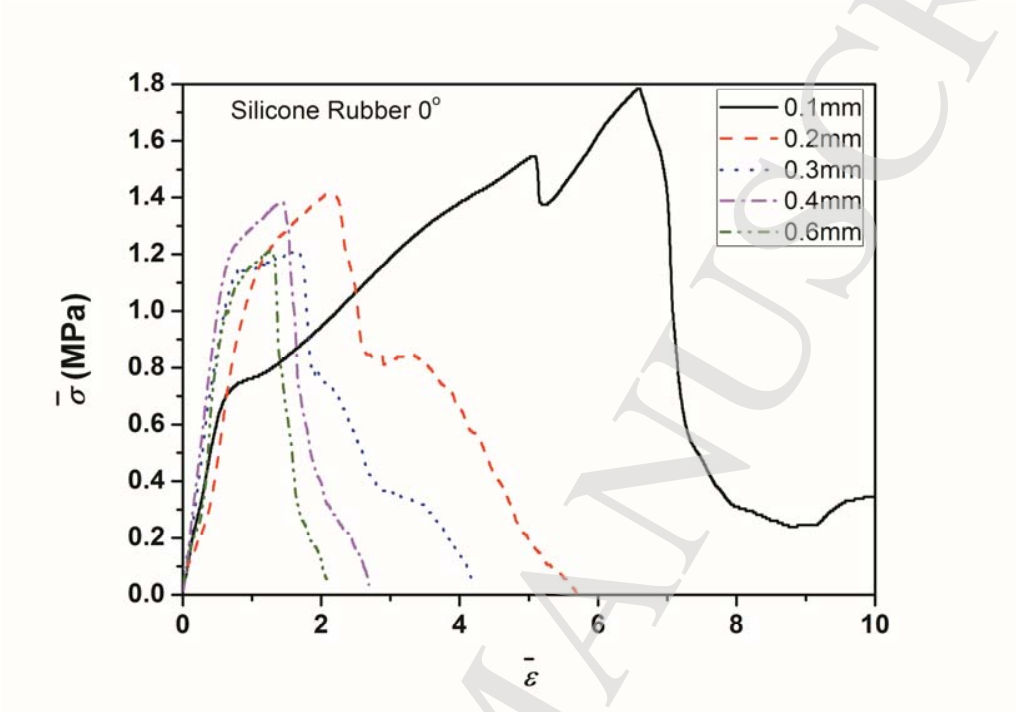


Fig. 8. Relations of average stress and average strain for varying adhesive layer thickness and given angle of adhesive interface, 0 degree.

Based on the relationships between the average normal stress- strain and the average shear stress-strain of the bonded interface, as shown in Figure 7 and Figure 8, we can further obtain the strength failure surface of the maximum normal stress and the maximum shear stress, as shown in Figure 9. It can be seen from Figure 9 that the strength failure surface of the bonded system is closely related to the thickness of the adhesive layer, and has a strong scale sensitivity. For the same bond thickness, average ultimate failure stresses for various scarf angles are on a circle, approximately, circle radius shrinks as bond thickness increases. In other words, for joints of the same bond thickness, external force per unit areas is nearly the same when joints fail, which provides strength predictions for metal / silicone rubber / metal bond systems that can be easily applied. Through some experimental results, it can be generalized to predict the strength failure load of the general scarf angle. Most of the experimental points are near the arc, and several points have a certain deviation.

For the sake of comparison, we also plot the strength points [Yang *et al*., 2014] of single lap specimens of the same material in Figure 9 (approximately to the 90 degree scarf angle). It should be pointed out that although the single lap joint test is a different test method from present test method, however both test methods have an obvious connection to some extent when scarf angle tends to 90 degree. In addition, the single lap joint was made from the same aluminum alloy and silicone rubber, and it was made under the same environmental conditions using the same manufacturing process. When the single lap joint is loaded on the testing machine, the adhesive layer is mainly subjected to the shear load, which is approximately to the 90 degree scarf angle.

It is interesting to note that the strength points of single lap joints [Yang *et al*., 2014] are also on this arc, approximately. This indicates that different experimental models have some relevance in some cases. The single lap joint can be considered to some extent as the limit of the scarf specimen (the bonding interface angle tends to be 90 degrees).

It can be seen from Figure 9 that the arc radius corresponding to 0.1 mm and 0.2mm of the adhesive layer thickness is obviously larger than that of the other adhesive layer thicknesses, which shows that when the adhesive layer thickness is very thin, the strength tends to increase sharply. The maximum tensile and shear strengths of the silicone rubber based on the standard samples are 0.33 MPa and 0.55 MPa, respectively [Yang *et al*., 2014]. However, in the present study, the ultimate tensile and shear strengths of silicone rubber bonded interface reach 2–5 times the standard sample strength, due to the metal adherend constraint. Its physical mechanism needs to be analyzed from the cross-scale mechanics theory, and we will conduct a systematic and in-depth study in the future.

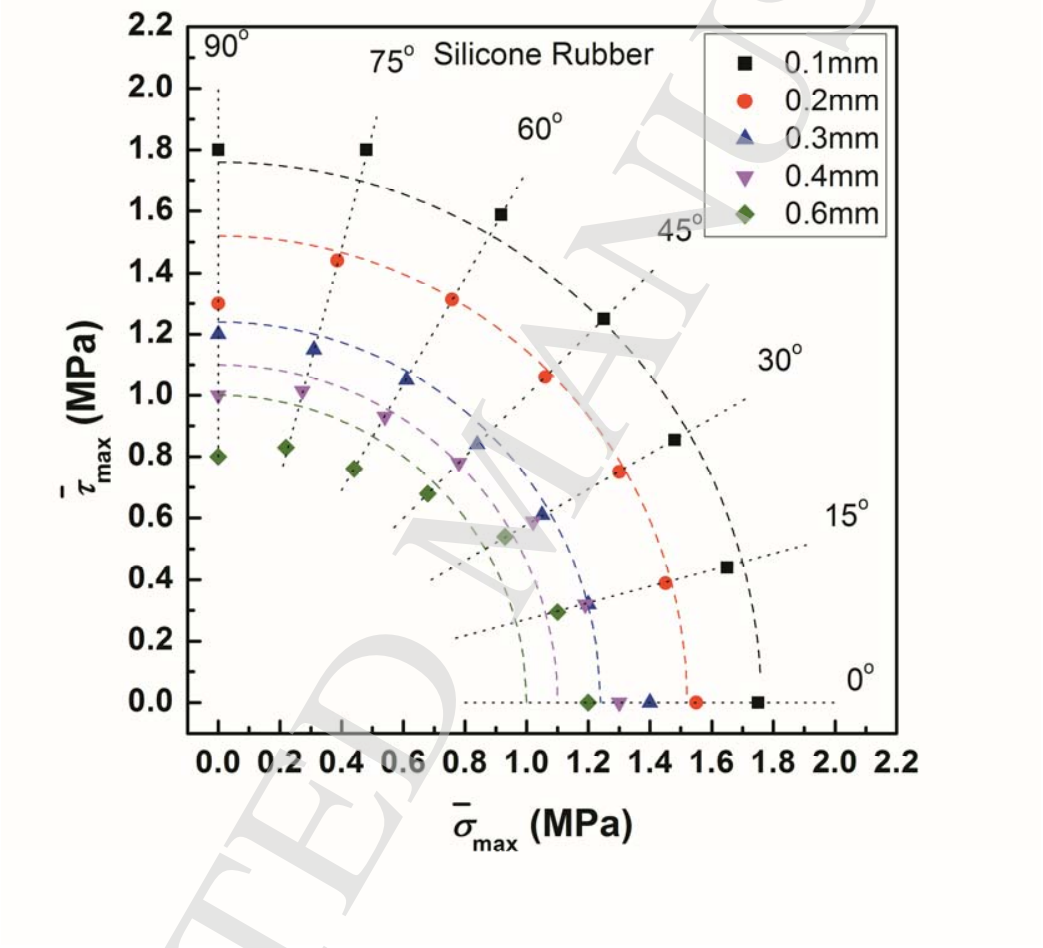


Fig. 9. Strength failure surface of adhesive interface.

## 5. Characterization of the Fracture Energy of the Bonded Interface for the Aluminum Alloy / Silicone Rubber / Aluminum Alloy System

In order to characterize the fracture energy of the bonded interface based on the previous experimental results, we give the expression of fracture toughness in the elastic range as follows

$$\Gamma(\theta)=\left(\frac{\bar{\tau}_c^{\,2}}{2G}+\frac{\bar{\sigma}_c^{\,2}}{2E}\right)*t \tag{5}$$

where $G$ and $E$ are the shear modulus and Young's modulus, respectively, $(\bar{\sigma}_c, \bar{\tau}_c)$ are the elastic limits of the average normal stress and the average shear stress, respectively.

Therefore, according to experimental results shown in Figures 7-9 and by using Eq. (5), we can obtain the interfacial elastic fracture energy as shown in Figure 10. As can be seen from Figure 10, the elastic fracture energy of the bonding interface of the metal / silicone rubber / metal system increases with the increases of the thickness of the adhesive layer and the scarf angles. Specifically, it is worth of noting that the elastic fracture energy is strong size effect on the adhesive layer thickness when it is smaller than 200 micron. The hierarchical property of the fracture energy for the adhesive system still needs to be further investigated.

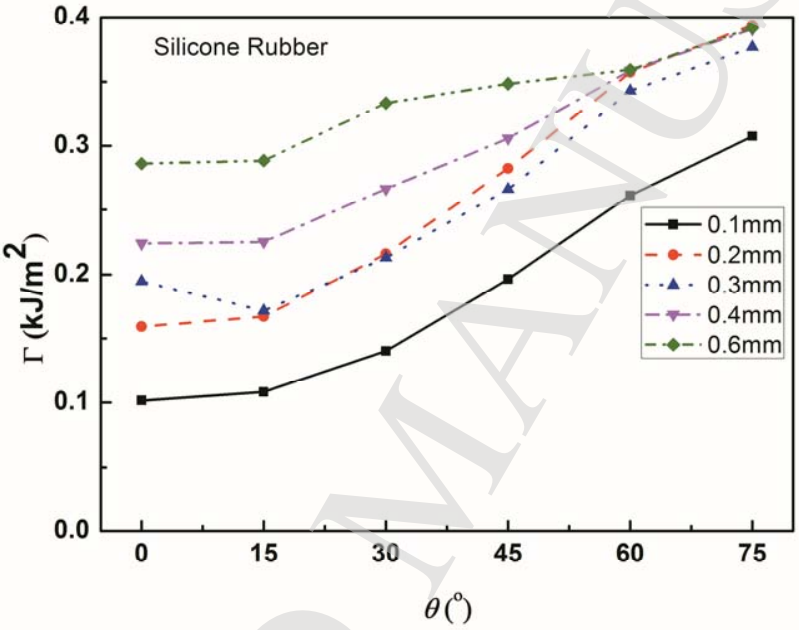


Fig. 10. Elastic fracture energy of adhesive interface.

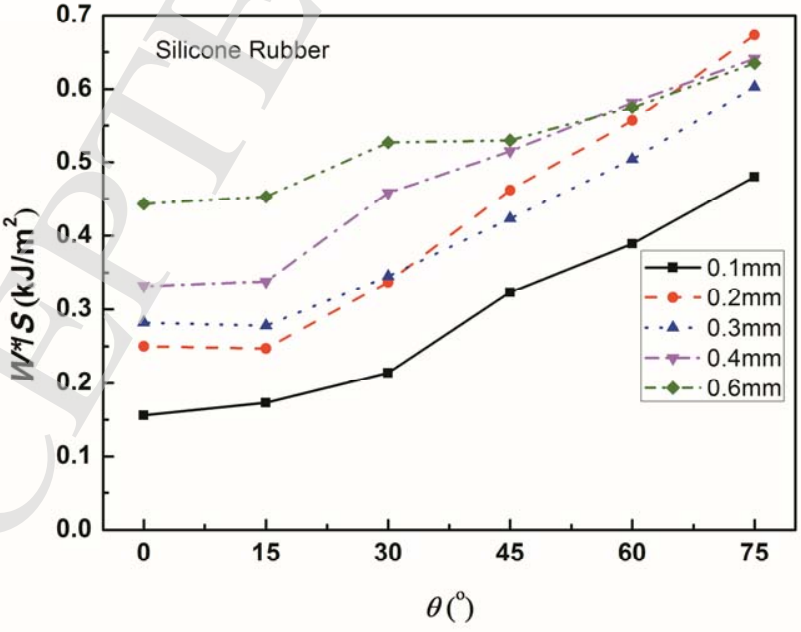

Fig. 11. Elastic energy release rate of metal/ silicone rubber adhesive system.

For comparison, we can also directly obtain the energy release rate $w = W^*/S$ of the bonding system of the aluminum alloy / silicone rubber / aluminum alloy through dividing the area (total elastic strain energy) of the elastic part under the load-displacement curve (see Figure 3-4) by the bonding area, where $W^*$ is the total elastic energy of the system and $S$ is the area of the adhesive layer. The result is shown in Figure 11. It can be seen from Figure 11 that the energy release rate of elastic part of the bonding system increases with the increase of the thickness of the adhesive layer and the scarf angle. Comparing Figure 10 and Figure 11, we can see that the elastic failure energy per unit area is about 65% of the total elastic energy release rate, it is to say that about 35% the energy release rate will be consumed in the area of the metal rod with holes and the inelastic deformation of the adhesive layer, which also needs more in-depth study and discussion.

It is worth noting that the failure strength and the interface fracture have strong scale effects when the thickness of the adhesive layer is below millimeter, especially when the thickness of the adhesive layer is close to 100 microns, the scale effect is extremely strong. The main reason for the scale effect is that when the thickness of the adhesive layer is very small, the tri-axial stress in the adhesive layer increases sharply to cause a high strain gradient effect near the interface. There are a number of documents that have discussed the scale effect on the failure strength and interfacial fracture. For example, the literature [Wei *et al*., 2008] discussed the problem of scale effect of adhesive thickness on film tearing problem, and the literature [Li *et al*., 2017] discussed the problem of scale effect of epoxy adhesive thickness on the bonding system.

## 6. Further Discussion

The schematic diagram of the linear model is shown in Figure 6.

The volume of the adhesive layer is given by

$$V = \frac{At}{\cos\theta} \tag{6}$$

The elastic strain energy of the adhesive can be given as

$$U = \int_V \frac{\bar{\sigma}^2}{2E} dV + \int_V \frac{\bar{\tau}^2}{2G} dV \tag{7}$$

Simplifying the above expression by using formulas (1) and (2), we can get

$$U = \frac{tF^2 \cos\theta}{2AE}\left(1 + \sin^2\theta + 2\upsilon \sin^2\theta\right) \tag{8}$$

A certain proportion of external force work is converted into elastic strain energy, we get

$$U = C^* W = C^* \frac{Fd}{2} \tag{9}$$

where $C$ is a constant. For elastic case $C$ value is about unity because the Young's modulus of aluminum alloy is much larger than that of the adhesive layer materials. The slope of elastic part of the force-displacement curve is derived as

$$k = \frac{F}{d} = C^* \frac{AE}{t\cos\theta(1 + \sin^2\theta + 2\upsilon \sin^2\theta)} \tag{10}$$

A dimensionless quantity is extracted

$$k_1 = \frac{kt}{AEC} = \frac{1}{\cos\theta(1 + \sin^2\theta + 2\upsilon \sin^2\theta)} \left(0^o \le \theta < 90^o\right) \tag{11}$$

$k_1$ is plotted in Figure 12.

In Figure 12, $k_1$ decreases first and then increases. As the Poisson's ratio increases, the position of the curve declines slightly. $k_1$ reaches the minimum at about 45 degrees and then $k_1$ increases as scarf angle increases until it becomes infinite.

We also find that

$$\frac{\bar{\sigma}}{\bar{\varepsilon}} = \frac{\bar{\tau}}{\bar{\gamma}} = \frac{Ft}{dA}\cos\theta = \frac{CE}{1+\sin^2\theta + 2\upsilon\sin^2\theta} \tag{12}$$

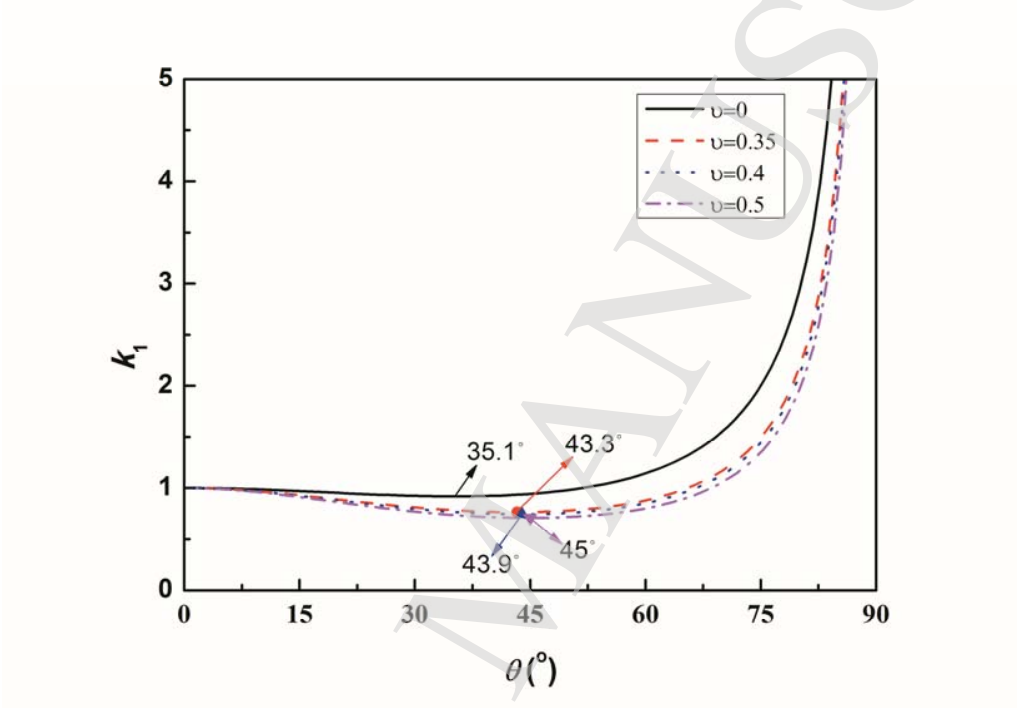


Fig. 12. $k_1$ changes with $\theta$ (The points with arrows are extreme points).

Using this model we can explain the phenomena mentioned above. In Figure 13, the curves containing the ascending and descending segments are the experimentally obtained curves. Those rays are the slope curves given by Eq. (10), wherein the constant takes 65 percent. The slope of the load-displacement curve decreases as scarf angle increases to about 45 degrees and then increases as the angle continues to increase, which shows a certain agreement with the regularity in Figure 12. The slopes of the 45 degree samples are the lowest and the slopes of the 75 degrees samples are higher than the slopes of the 0 degree samples. Very similar trends have also been found on other silicone rubber specimens having bond thickness between 0.1 mm and 0.6 mm.

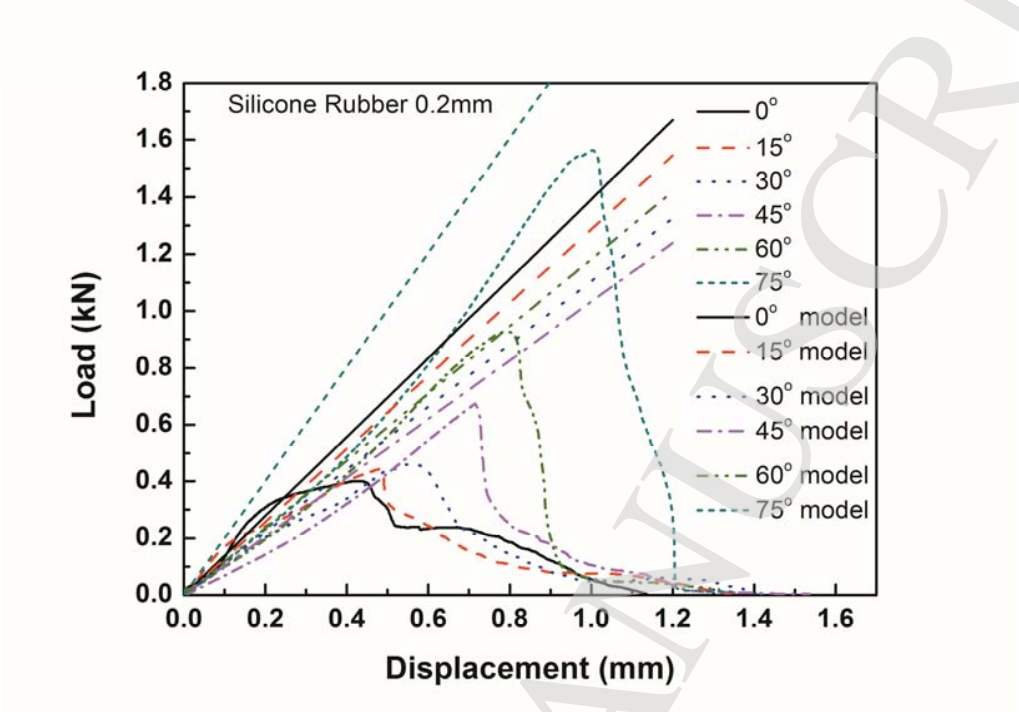


Fig. 13. Load-displacement curves of scarf adhesive joints with the same bond thickness（0.2mm）but different scarf angles.

In Figure 14, the curves containing the ascending and descending segments are the experimentally obtained curves. Those rays are the slope curves given by Eq. (10), wherein the constant takes 65 percent. The slope of silicone rubber sample is approximately inversely proportional to the bond thickness, which is in good agreement with the model. Very similar trends have also been found on other silicone rubber specimens having scarf angles between 0 degree and 75 degrees.

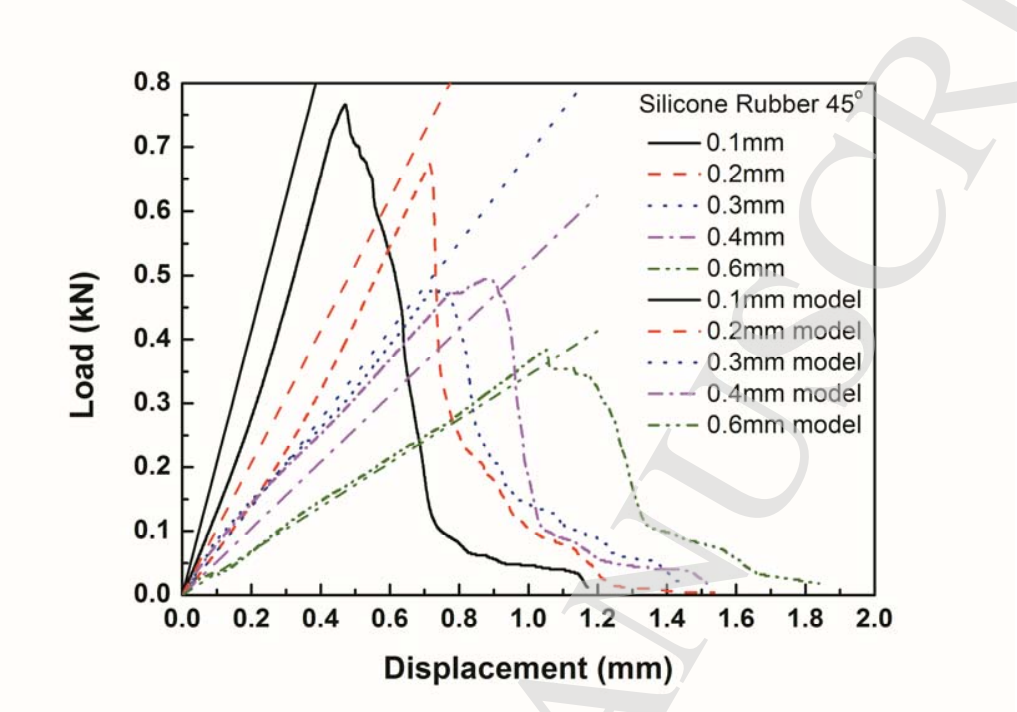


Fig. 14. Load-displacement curves of scarf adhesive joints with the same scarf angle（45 degrees）but different bond thickness.

In Figure 7, the slope of the stress-strain curve decreases as scarf angle increases, which is in good agreement with Eq. (12). Very similar trends have also been found on other silicone rubber specimens having bond thickness between 0.1 mm and 0.6 mm.

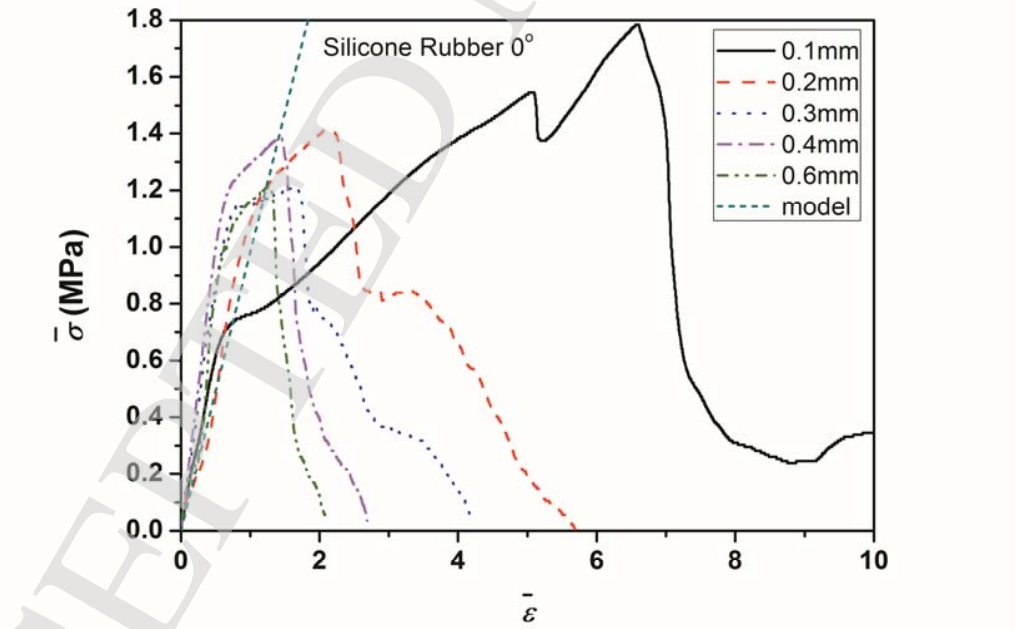


Fig. 15. Stress-strain curves of 0 degree scarf adhesive joints with the same scarf angle but different bond thickness.

In Figure 15, the curves containing the ascending and descending segments are the experimentally obtained curves. The ray is the slope curve given by Eq. (12), wherein the constant takes 65 percent. The slopes of silicone rubber samples with 0 degree scarf angle are nearly the same, which is in good agreement with the model. Very similar trends have also been found on other silicone rubber specimens having bond thickness between 0 degree and 75 degrees.

In above sections, our experimental analyses of the strength, toughness and failure mechanisms for the metal/adhesive bonding system are based on a combined model of simple tension with simple shear shown in Figure 6. In addition, it should be interesting to investigate the relation of the equivalent stress and strain. For the metal/silicon rubber /metal system, if we still assume the unidirectional stress field in the adhesive layer, the equivalent stress and strain can be expressed as

$$\sigma^e = \frac{F}{A}, \quad \varepsilon^e = \frac{d}{t}\cos\theta \tag{13}$$

Therefore, the equivalent stress-strain curves ( $\sigma^e \sim \varepsilon^e$ curves) are very similar to the load-displacement curves, as shown in Figures 2~ 4, besides the changes of the horizontal coordinates.

## 7. Concluding Remarks

In the present research, we have carried out experimental study on the toughness mechanism and failure behavior systematically for the metal / silicone rubber / metal bonding system. For the aluminum alloy round rod and the aluminum alloy round rod bonded through the silicone rubber adhesive layer, we have investigated the tensile deformation and failure characteristics of scarf joints and the dependence of interface failure load on both the thickness of the adhesive layer and the scarf angle. Through introducing the concepts of average normal stress, average shear stress, average normal strain and average shear strain in the bonding interface layer, the interface failure strength have been measured. The relationship between interface strength and scarf angle and bond thickness have been developed, and then the strength failure surface of the system of the aluminum alloy / silicone rubber adhesive layer / aluminum alloy and the fracture energy of the bonded interface and the energy release rate of the bonded system have been also obtained. The following main conclusions are obtained:

- Tensile failure of the aluminum alloy / silicone rubber adhesive layer / aluminum alloy system is characterized by ductile failure, and the failure is often taken place inside the adhesive layer. Failure load and strength show a strong scale effect on a layer thickness of the order of hundred microns. The bonding strength increases significantly with decreasing thickness of the adhesive layer. At the same time, the bonding load depends critically on the scarf angle.
- The tensile bonding strength at the interface of the silicone rubber adhesive layer decreases with the increase of the scarf angle, while the shear bonding strength increases with the increase of the scarf angle of the adhesion interface. The mixed failure points of tensile bonding strength and shear bonding strength are located on the same circle of the strength failure surface.
- The fracture energy of the bonding interface of the aluminum alloy / silicone rubber / aluminum alloy system show a strong scale effect on the scale of the bond thickness of hundred microns. With the increase of the bond thickness, the interfacial fracture energy can be obviously increased. At the same time, the interfacial fracture energy increases significantly with the increase of the scarf angle.
- When damage of the aluminum alloy / silicone rubber adhesive layer / aluminum alloy bonding system takes place, bonding interfacial fracture energy is accounted for the system's 65% overall energy release rate. A part of the energy is released by deformation of the metal rod and inelastic deformation of the adhesive layer during the system failure.

The above results provide a scientific basis for understanding the toughness and failure mechanism of metal bonding system, and have important guiding significance for the optimization design and performance evaluation of metal bonding system.

**Acknowledgments**

This work was supported by the National Natural Science Foundation of China through Grant no. 11432014; 11672301; 11521202; 11672296; 11372318.

**References**

Afendi, M., Majid, M. S. A., Daud, R., Rahman, A. A. and Teramoto, T. [2013] "Strength prediction and reliability of brittle epoxy adhesively bonded dissimilar joint," International Journal of Adhesion and Adhesives 45(2), 21-31.

Afendi, M., Teramoto, T. and Bakri, H. B. [2011] "Strength prediction of epoxy adhesively bonded scarf joints of dissimilar adherends," *International Journal of Adhesion and Adhesives* **31**(6), 402-411.

Arcan, L., Arcan, M. and Daniel, I. [1987] "SEM fractography of pure and mixed mode inter-laminar fracture in graphite/epoxy composites," *ASTM Technologies* **948**, 41–67.

Ascione, F. [2009] "Mechanical behavior of FRP adhesive joints: A theoretical model," *Composites Part B: Engineering* **40**, 116–124.

Banea, M. D., da Silva, L. F. M. and Campilho, R. D. D. G. [2014] "Effect of temperature on the shear strength of aluminium single lap bonded joints for high temperature applications," *Journal of Adhesion Science and Technology* **28**, 1367-1381.

Bendemra, H., Compston, P. and Crothers, P. J. [2015] "Optimisation study of tapered scarf and stepped-lap joints in composite repair patches," *Composite Structures* **130**, 1-8.

Chaudhuri, R. A. and Sou-Hsiung, J. C. [2009] "Three-dimensional asymptotic stress field in the vicinity of an adhesively bonded scarf joint interface," *Composite Structures* 8**9**(3), 475-483.

Chiu, S. H. J. and Chaudhuri, R. A. [2011] "A three-dimensional eigenfunction expansion approach for singular stress field near an adhesively-bonded scarf joint interface in a rigidly-encased plate," *Engineering Fracture Mechanics* **78**(10), 2220-2234.

Choupani, N. [2008a] "Interfacial mixed-mode fracture characterization of adhesively bonded joints," *International Journal of Adhesion and Adhesives* **28**(6), 267-282.

Choupani, N. [2008b] "Mixed-mode cohesive fracture of adhesive joints: Experimental and numerical studies," *Engineering Fracture Mechanics* **75**(15), 4363-4382.

Dai, J. G., Ueda, T. and Sato, Y. [2005] "Development of the nonlinear bond stress-slip model of fiber reinforced plastics sheet-concrete interfaces with a simple method," *Journal of Composites for Construction* **9**, 52–62.

Gacoin, A., Lestriez, P., Assih, J., Objois, A. and Delmas, Y. [2009] "Comparison between experimental and numerical study of the adhesively bonded scarf joint and double scarf joint: Influence of internal singularity created by geometry of the double scarf joint on the damage evolution," *International Journal of Adhesion and Adhesives* **29**, 572–579.

Goglio, L., Rezaei, M. and Rossetto, M. [2014] "Moisture degradation of open-faced single lap joints," *Journal of Adhesion Science and Technology* **28**, 1382-1393.

Grant, L. D. R. Adams, R. D. da Silva, L. F. M. [2009] "Effect of the temperature on the strength of adhesively bonded single lap and T joints for the automotive industry," *International Journal of Adhesion and Adhesives* **29**, 535–542.

Grant, L. D. R., Adams, R. D. and da Silva, L. F. M. [2009] "Experimental and numerical analysis of single-lap joints for the automotive industry," *International Journal of Adhesion and Adhesives* **29**, 405–413.

Groth, H. L. [1988] "Prediction of failure loads of adhesive joints using the singular intensity factors," *Fracture Mechanics: Eighteenth Symposium: ASTM STP* **945**, 278–284.

Higgins, A. [2000] "Adhesive bonding of aircraft structures," *International Journal of Adhesion and Adhesives* **20**, 367–376.

Imanaka, M., Fujinami, A. and Suzuki, Y. [2000] "Fracture and yield behavior of adhesively bonded joints under triaxial stress conditions," *Journal of Materials Science* **35**, 2481–2491.

Jen, Y. M. [2012] "Fatigue life evaluation of adhesively bonded scarf joints," *International Journal of Fatigue* **36**(1), 30-39.

Kahraman, R., Sunar, M. and Yilbas, B. [2008] "Influence of adhesive thickness and filler content on the mechanical performance of aluminum single-lap joints bonded with aluminum powder filled epoxy adhesive," *Journal of Materials Processing Technology* **205**, 183-189.

Kim, M. K., Elder, D. J., Wang, C. H. and Feih, S. [2012] "Interaction of laminate damage and adhesive disbonding in composite scarf joints subjected to combined in-plane loading and impact," *Composite Structures* **94**(3), 945-953.

Kinloch, A. J. [1987] "Adhesion and Adhesives: Science and Technology," London, Chapman and Hall.

Liao, L., Sawa, T. and Huang, C. [2014] "Numerical analysis on load-bearing capacity and damage of double scarf adhesive joints subjected to combined loadings of tension and bending," *International Journal of Adhesion and Adhesives* **53**(18), 65-71.

Li, H., Zhang, P. and Cheng, Y. Q. [2013] "Research effects of metal pretreatment on the bonding strength of metal/polymer interface," *Fiber Reinforced Plastics/Composites* **4**, 51-54. (in Chinese)

Li, J., Liang, L. H., Liu, X. M., Ma, H. S., Song, J. R. and Wei, Y. G. [2017] "Experimental investigations of strength, toughness and failure mechanism of the metal/epoxy/metal adhesive system," *Chinese Journal of Theoretical and Applied Mechanics* **49**(6), 1213-1222. (in Chinese)

Loureiro, A. L., da Silva, L. F. M., Sato, C. and Figueiredo, M. A. V. [2010] "Comparison of the Mechanical Behavior Between Stiff and Flexible Adhesive Joints for the Automotive Industry," The Journal of Adhesion 86, 765–787.

Nakano, H., Omiya, Y. Sekiguchi, Y. and Sawa T. [2014] "Three-dimensional FEM stress analysis and strength prediction of scarf adhesive joints with similar adherends subjected to static tensile loadings," *International Journal of Adhesion and Adhesives* **54**(5), 40-50.

Nakano, H., Sekiguchi, Y. and Sawa, T. [2013] "FEM stress analysis and strength prediction of scarf adhesive joints under static bending moments," *International Journal of Adhesion and Adhesives* **44**, 166–173.

Stamoulis, G., Carrere, N., Cognard, J. Y., Davies, P. and Badulescu, C. [2016] "Investigating the fracture behavior of adhesively bonded metallic joints using the Arcan fixture," *International Journal of Adhesion and Adhesives* **66**, 147-159.

Suzuki, Y. [1985] "Adhesive Tensile Strengths of Scarf and Butt Joints of Steel Plates : 2nd Report, Relation between Mechanical Properties of Adhesive and Fracture Criteria of Joints," *Bulletin of Jsme* **28**(463), 2575-2584.

Suzuki, Y. [1987] "Adhesive Tensile Strengths of Scarf and Butt Joints of Steel Plates (Relation Between Adhesive Layer Thicknesses and Adhesive Strengths of Joints) : Solid-Mechanics, Strength of Materials," *Nihon Kikai Gakkai Ronbunshu A Hen/transactions of the Japan Society of Mechanical Engineers Part A* **53**(487), 514-522.

Wang, C. H. and Rose, L. R. F. [1997] "Determination of triaxial stresses in bonded joints," *International Journal of Adhesion and Adhesives* **17**, 17–25.

Wang, X., Lin, J. P. and Wan, H. L. [2017] "Research progress in effect of aluminum surface properties on adhesively bonded performance," *Journal of Materials Engineering* **45**(8), 123-131. (in Chinese)

Wei, Y. and Zhao, H. [2008] "Peeling experiments of ductile thin films along ceramic substrates – Critical assessment of analytical models," *International Journal of Solids & Structures* **45**(13), 3779-3792.

Wu, Z. S., Yuan, H. and Niu, H. D. [2002] "Stress transfer and fracture propagation in different kinds of adhesive joints," *Journal of Engineering Mechanics-ASCE* **128**, 562–573

Xu, W., Chen, L., Zhang, Q. C. and Wei, Y. G. [2012] "Mechanical behavior and characterization of bonding interface," *Scientia Sinica Technologica* **42**(12), 1361-1376. (in Chinese)

Yang S., Xu W., Liang L. H., Wang, Z. Q. and Wei, Y. G. [2014] "An experimental study on the dependence of the strength of adhesively bonded joints with thickness and mechanical properties of the adhesives," *Journal of Adhesion Science and Technology* **28**, 1055-1071.

Zhang, J. and Jia, H. [2016] "Influence of cohesive zone models shape on adhesively bonded joints," *Chinese Journal of Theoretical and Applied Mechanics* **48**(5), 1088-1095. (in Chinese)

Zhan, Z., Meng, Q., Hu, W., Sun, Y., Shen, F. and Zhang, Y. [2017] "Continuum damage mechanics based approach to study the effects of the scarf angle, surface friction and clamping force over the fatigue life of scarf bolted joints," *International Journal of Fatigue* **102**.

**Figure Caption:**

Figure 1. Specimen size (mm).

Figure 2. Load-displacement curve of typical specimen of the aluminum alloy/ silicone rubber/ aluminum alloy.

Figure 3. Load-displacement curves for varying angle of adhesive interface and given adhesive layer thickness.

Figure 4. Load-displacement curves for varying adhesive layer thickness and given angle of adhesive interface.

Figure 5. Failure loads vary with scarf angle.

Figure 6. Sketch Figures of deformation and average stresses on the adhesive interface. (a)Sketch of deformation; (b)Sketch of average stresses.

Figure 7 Relations of average stress and average strain for varying angle of adhesive interface and given adhesive layer thickness. (a)Average normal stress vs average normal strain; (b) Average shear stress vs average shear strain.

Figure 8. Relations of average stress and average strain for varying adhesive layer thickness and given angle of adhesive interface, 0 degree.

Figure 9. Strength failure surface of adhesive interface.

Figure 10. Fracture energy of adhesive interface.

Figure 11. Energy release rate of metal/ silicone rubber adhesive system.

Figure 12. $k_1$ changes with $\theta$ (The points with arrows are extreme points).

Figure 13. Load-displacement curves of scarf adhesive joints with the same bond thickness（0.2mm） but different scarf angles.

Figure 14. Load-displacement curves of scarf adhesive joints with the same scarf angle（45 degrees） but different bond thickness.

Figure 15. Stress-strain curves of 0 degree scarf adhesive joints with the same scarf angle but different bond thickness.